Nuclear physics for geo-neutrino studies

Gianni Fiorentini,[1,2] Aldo Ianni,[3] George Korga,[3] Marcello Lissia,[4,*] Fabio Mantovani,[1,2,5] Lino Miramonti,[6,7] Lothar Oberauer,[8] Michel Obolensky,[9] Oleg Smirnov,[10] and Yury Suvorov[3]

[1]*Dipartimento di Fisica, Università degli Studi di Ferrara, I-44100 Ferrara, Italy*
[2]*Istituto Nazionale di Fisica Nucleare, Sezione di Ferrara, I-44100 Ferrara, Italy*
[3]*Istituto Nazionale di Fisica Nucleare, Laboratori Nazionali del Gran Sasso, I-67010 Assergi, Italy*
[4]*Istituto Nazionale di Fisica Nucleare, Sezione di Cagliari, I-09042 Monserrato, Italy*
[5]*Centro di GeoTecnologie, I-52027 San Giovanni Valdarno, Italy*
[6]*Dipartimento di Fisica, Università degli Studi di Milano, I-20133 Milano, Italy*
[7]*Istituto Nazionale di Fisica Nucleare, Sezione di Milano, I-20133 Milano, Italy*
[8]*Physik Department, Technische Universität Muenchen, D-85747 Garching, Germany*
[9]*Laboratoire AstroParticule et Cosmologie, F-75231 Paris CEDEX 13, France*
[10]*Joint Institute for Nuclear Research, RU-141980 Dubna, Russia*

(Received 24 August 2009; published 4 March 2010)

Geo-neutrino studies are based on theoretical estimates of geo-neutrino spectra. We propose a method for a direct measurement of the energy distribution of antineutrinos from decays of long-lived radioactive isotopes. We present preliminary results for the geo-neutrinos from ^{214}Bi decay, a process that accounts for about one-half of the total geo-neutrino signal. The feeding probability of the lowest state of ^{214}Bi—the most important for geo-neutrino signal—is found to be $p_0 = 0.177 \pm 0.004$ (stat) $^{+0.003}_{-0.001}$ (sys), under the hypothesis of universal neutrino spectrum shape (UNSS). This value is consistent with the (indirect) estimate of the table of isotopes. We show that achievable larger statistics and reduction of systematics should allow for the testing of possible distortions of the neutrino spectrum from that predicted using the UNSS hypothesis. Implications on the geo-neutrino signal are discussed.

DOI: 10.1103/PhysRevC.81.034602 PACS number(s): 14.60.Pq, 23.40.Bw, 92.20.Td

I. INTRODUCTION

Geo-neutrinos, the antineutrinos from the progenies of U, Th, and ^{40}K decays in the Earth, bring to the surface information from the whole planet concerning its content of radioactive elements. Their detection can shed light on the sources of the terrestrial heat flow of the Earth, on its present composition, and on its origins.

Although geo-neutrinos were conceived very long ago, only recently have they been considered seriously as a new probe of our planet's interior, as a consequence of two fundamental advances that occurred in the last few years: the development of large, extremely low background neutrino detectors and progress in understanding neutrino propagation. From the theoretical point of view, the links between the geo-neutrino signal and the total amount of natural radioactivity in the Earth have been analyzed by several groups. Various reference models [1–3] for geo-neutrino production have been presented in the literature; some of these models have been refined with geological and geochemical studies of the regions surrounding the detectors [4]. The KamLAND [5,6] and Borexino [7,8] collaborations are collecting geo-neutrino data, while several planned experiments (e.g., SNO+, LENA, HANOHANO, EARTH, among others) have geo-neutrino measurements among their primary goals. A recent review is presented in Ref. [9].

This activity has to be complemented with some deepening of the nuclear physics that is at the basis of geo-neutrino detection and that is crucial for interpreting future geo-neutrino data. The aim of this article is to discuss the uncertainties of some nuclear physics parameters that enter into the interpretation of the geo-neutrino signal and to provide a framework for an experimental determination of these parameters.

In all experiments that use hydrocarbons as detection media, either running or in preparation, the reaction for geo-neutrino detection is the inverse β decay on free protons:

$$\bar{\nu}_e + p \rightarrow e^+ + n - 1.806\ \text{MeV}. \tag{1}$$

The signal is estimated from the cross section $\sigma(E_\nu)$ of Eq. (1) and from the decay spectra $f(E_\nu)$ of geo-neutrinos produced in each β decay along the decay chains, the relevant quantity being the specific signals defined as

$$s_i = \int_{E_0}^{E_{\max}} dE_\nu \sigma(E_\nu) f_i(E_\nu), \tag{2}$$

where $E_0 = 1.806$ MeV is the threshold energy for reaction Eq. (1), $E_{\max}$ is the maximal geo-neutrino energy, and the spectrum $f(E_\nu)$ is normalized to one geo-neutrino[1]:

$$\int_0^{E_{\max}} dE_\nu f(E_\nu) = 1. \tag{3}$$

*marcello.lissia@ca.infn.it

[1]A detector with N_p free protons will collect a signal rate $S = N_p \sum_i \Phi_i s_i$, where Φ_i are the incoming fluxes of geo-neutrinos from the ith β decay in the chain and s_i are the corresponding specific signals.

TABLE I. Effective transitions in the ^{238}U chain from Ref. [9]. In bold are the reactions that give most of the signal. For each decay, the table shows the probability, the maximal antineutrino energy, the intensity I_k, its error ΔI_k, and type and percentage contributions to the uranium geo-neutrino signal and to the (U + Th) geo-neutrino signal. For this last column, it is assumed that the chondritic ratio for the masses (Th/U = 3.9), which implies that 79% of the geo-neutrino signal comes from uranium.

$i \to j$	$R_{i,j}$	$E_{\max}$ (keV)	I_k	ΔI_k	Type (%)	S_{U} (%)	S_{tot}
$^{234}\mathrm{Pa}_m \to {}^{234}\mathrm{U}$	**0.9984**	**2268.92**	**0.9836**	**0.002**	**first forbidden** $(0^-) \to 0^+$	**39.62**	**31.21**
$^{214}\mathrm{Bi} \to {}^{214}\mathrm{Po}$	**0.9998**	**3272.00**	**0.182**	**0.006**	**first forbidden** $1^- \to 0^+$	**58.21**	**45.84**
		2662.68	0.017	0.006	first forbidden $1^- \to 2^+$	1.98	1.55
		1894.32	0.0743	0.0011	first forbidden $1^- \to 2^+$	0.18	0.14
		1856.51	0.0081	0.0007	first forbidden $1^- \to 0^+$	0.01	0.01

It is important to observe that the specific signal is affected by unknown uncertainties. In fact, whereas $\sigma(E_\nu)$ is affected by uncertainties of less than 1 percent [10,11], it is difficult to assess the accuracy of $f(E_\nu)$, which is determined from rather indirect measurements and questionable theoretical assumptions. Our goal is to provide a framework for a direct measurement of $f(E_\nu)$ so that the accuracy of the specific signal can be established.

II. WHY SHOULD GEO-NEUTRINO SPECTRA BE MEASURED?

Geo-neutrinos are produced through pure β and β-γ processes:

$$X \to X' + e + \bar{\nu}_e,$$
$$X \to X'^{*} + e + \bar{\nu}_e,$$
$$\searrow$$
$$X' + n + \gamma.$$

To determine the geo-neutrino decay spectra $f(E_\nu)$, one has to know: (i) the feeding probabilities p_n of the different energy states of the final nucleus and (ii) the shape of the neutrino spectrum for each transition. Let us discuss in some detail the procedures and assumptions used for deriving these quantities.

Feeding probabilities are derived from measurements of the intensities $I_\gamma^{m,n}$ of the γ lines. These are corrected for internal conversion to derive the transition probabilities from level m to n:

$$I^{m,n} = I_\gamma^{m,n}(1 + \alpha^{m,n}). \tag{4}$$

The internal conversion coefficients $\alpha^{m,n}$ are obtained by theoretical calculations. In general they are of order 10^{-2}, unless selection rules forbid or inhibit the γ emission.[2]

The feeding probabilities for the excited states are then obtained with a subtraction procedure as the difference between the intensities of outgoing and ingoing transitions:

$$p_n = \sum_{m<n} I^{n,m} - \sum_{m>n} I^{m,n}. \tag{5}$$

The feeding probability of the lowest state, p_0, is obtained with the same subtraction procedure:

$$p_0 = 1 - \sum_{m>0} I^{m,0}. \tag{6}$$

This procedure implies that all transitions to the ground state that are not observed or taken into account are included in the feeding probability to the lowest energy state. In other words, p_0 is indirectly determined, whereas it is of special interest for our purposes: β transitions directly to the lowest energy state, the pure β's, produce the most energetic geo-neutrinos, and thus give the largest contribution to the specific signal.

For each transition, the shape of the neutrino spectrum is generally calculated assuming the well-known universal shape distribution. This expression (see Ref. [9]) corresponds to momentum-independent nuclear matrix elements (as for allowed transitions) and includes the effect of the bare Coulomb field of the nucleus through the relativistic Fermi function. Electron screening and nuclear finite size effects are not considered. Note that this same universal shape expression is used even for the forbidden transitions (see Tables I and II),

[2]An important case in this respect is the $E0$ transition of ^{214}Bi at 1415.8 keV, which occurs essentially through internal conversion.

TABLE II. Effective transitions in the ^{232}Th chain from Ref. [9]. In bold is the reaction that gives most of the signal. For each decay, the table shows the probability, the maximal antineutrino energy, the intensity I_k, its error ΔI_k, and type and percentage contributions to the thorium geo-neutrino signal and to the total (U + Th) geo-neutrino signal. For this last column, it is assumed that the chondritic ratio for the masses (Th/U = 3.9), which implies that 21% of the geo-neutrino signal comes from thorium.

$i \to j$	$R_{i,j}$	$E_{\max}$ (keV)	I_k	ΔI_k	Type (%)	S_{Th}	S_{tot}
$^{212}\mathrm{Bi} \to {}^{212}\mathrm{Po}$	**0.6406**	**2254**	**0.8658**	**0.0016**	**first forbidden** $1^{(-)} \to 0^+$	**94.15**	**20.00**
$^{228}\mathrm{Ac} \to {}^{228}\mathrm{Th}$	1.0000	2069.24	0.08	0.06	allowed $3^+ \to 2^+$	5.66	1.21
		1940.18	0.008	0.006	allowed $3^+ \to 4^+$	0.19	0.04

where momentum-dependent nuclear matrix elements can appear.

These observations suggest that the feeding probabilities need to be confirmed by different experimental techniques and that the electron decay spectrum needs to be experimentally tested.

III. TOWARD A DIRECT MEASUREMENT OF GEO-NEUTRINO DECAY SPECTRA

When the nucleus X decays, whatever the transition involved, energy conservation provides a connection between the neutrino energy E_ν, the kinetic energy of the electron T_e, and the total energy of the emitted γs E_γ:

$$Q = E_\nu + T_e + E_\gamma, \tag{7}$$

where $Q = M_X - M_{X'} - M_e$ is the Q value for the decay. To measure the geo-neutrino spectrum, one needs a calorimetric detector capable of measuring the visible energy deposited by electrons[3] and γs, $E_{\rm vis} = T_e + E_\gamma$. When measured decay events are displayed as a function of $E_{\rm vis}$, by mirror reflection, one immediately obtains the number of events as a function of neutrino energy at $E_\nu = Q - E_{\rm vis}$; as an example, see Fig. 1 for the decay spectrum of ^{214}Bi.

For such a measurement, one needs a detector that can collect the energy lost by both electrons and γs and that has a similar response to both particles. Essentially, this is a calorimetric measurement. In principle, it can be done with large bolometers [12], which have very good energy resolution but long dead times. A sufficiently large liquid scintillator detector is suitable for such measurements. Although energy resolution is limited, nevertheless, it can contain both electrons and γs, and significant statistics can be collected in a reasonable amount of time.

There are some limitations that should be considered when using a scintillator as a calorimeter. An ideal detector should provide the same response for γs and electrons with equal energy, independently of the positions where the particles are generated. In practice, however, the following should be considered:

(i) Even in a very large detector, the energy released as scintillation light from electrons and γs of the same energy are not the same. This difference becomes marked at low energy (see Fig. 2).
(ii) The γs can escape from a finite detector, thus releasing only a fraction of their energy.
(iii) The number of photons collected by the detector can depend on the position where they have been produced (because of absorption, optical coverage, etc.).

All these effects can be taken into account by using calibration measurements, by selecting events that occur in the inner part of the detector (to minimize corrections because of escaping γs), and with energy above a suitable threshold. The comparison between experimental spectra and theoretical predictions has to be implemented by means of a Monte Carlo simulation that accounts for the actual characteristics of the detector.

[3]Note that the energy deposited by conversion electrons is also included.

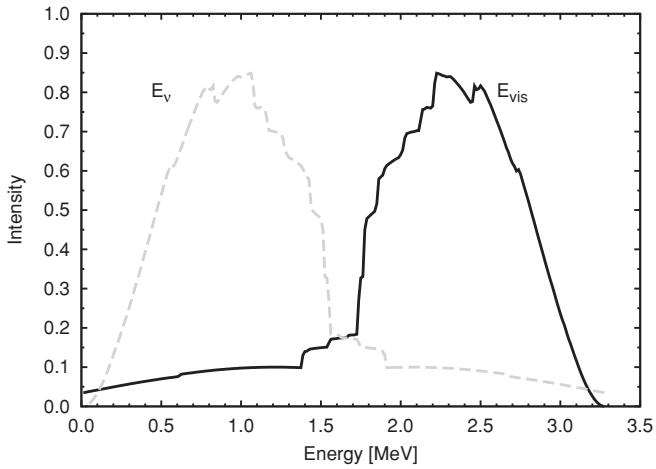

FIG. 1. The decay spectrum of ^{214}Bi as a function of the visible energy $E_{\rm vis}$ (solid line) and of the neutrino energy E_ν (dashed line).

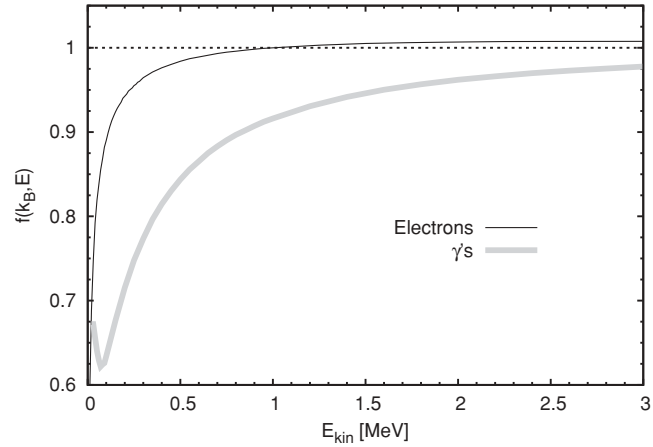

FIG. 2. Quenching factor for electrons and γs, for a Birks coefficient $k_B = 1.95 \cdot 10^{-3}$ cm MeV^{-1} (see the appendix). The quenching factor has been normalized so that is 1 for 1-MeV electrons.

IV. THE PROPOSED DETECTOR

We propose to exploit the potential of the Counting Test Facility (CTF), which is operational and available in the underground Istituto Nazionale di Fisica Nucleare Gran Sasso National Laboratory.

Like Borexino, the CTF design [13] is based on the principle of graded shielding (see Figs. 3 and 4). The active scintillation liquid in CTF is a 4-ton mass of pseudocumene enclosed in a transparent nylon sphere, the CTF vessel. Outside this vessel, there is a volume of ultrapure water enclosed in a second nylon sphere, the so-called CTF radon shroud, intended to prevent radon transport with thermal fluxes from the outside zones of the detector. A set of inward-facing photomultiplier tubes (PMT) is arrayed outside the shroud. The entire apparatus, surrounded by another volume of water, is contained in a

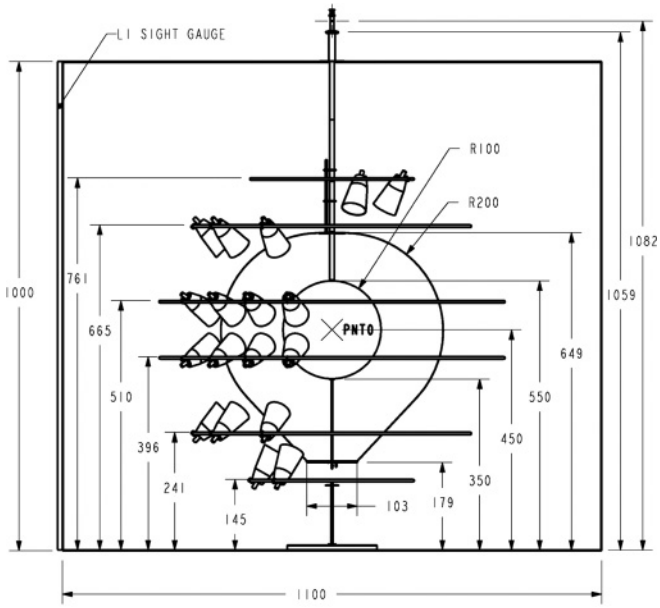

FIG. 3. Side view of the design of CTF. The vessel (labeled R100 in this drawing) and shroud (R200) are shown, as are the six rings of PMTs, the cylindrical tank, and the tubes used for filling and draining the vessel. The point PNT0 is the nominal center of the sphere of PMTs and of the CTF vessel. Dimensions are given in centimeters. Courtesy of the Borexino Collaboration.

cylindrical stainless tank. The bottom surface of the tank holds 16 upward-facing PMTs, used to tag the muons passing through the detector by means of the Cherenkov light in the water.

The facility is equipped with a rod system that can be used to insert a small, cylindrical quartz vial inside the CTF vessel. A suitable source, dissolved in the liquid scintillator, can be placed in the vial. Electrons are stopped inside the vial, and the scintillation light is propagated within CTF through the quartz (which is transparent to the near-UV wavelengths of scintillation light and has an index of refraction close to that of the scintillator), whereas γ conversion occurs inside the CTF inner vessel. The inward-facing PMTs outside the shroud can thus detect light originating from both electrons and γs.

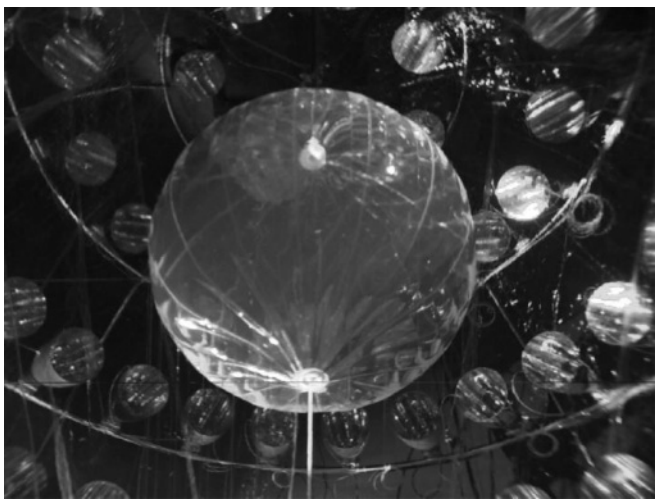

FIG. 4. A picture of the CTF viewed from below. Courtesy of the Borexino Collaboration.

A Monte Carlo code has been developed for CTF. It is described in Ref. [14] and in the appendix, with adjustments for our specific task.

V. WHAT HAS TO BE MEASURED?

Geo-neutrinos with energy above the threshold for reaction Eq. (1) arise only from the chains of ^{238}U and ^{232}Th. In particular, for ^{238}U, only three nuclides (^{234}Pa, ^{214}Bi, ^{210}Tl) contribute to the geo-neutrino signal. The contribution from ^{210}Tl is negligible because of its small occurrence probability, and the uranium contribution to the geo-neutrino signal comes from five β decays: one from ^{234}Pa and four from ^{214}Bi. Table I lists the effective transitions, that is, those that can produce antineutrinos with energy above the threshold E_0. In fact, 98% of the uranium signal arises from the two transitions to the ground state (in bold in Table I), and an accuracy better than 1% is achieved by adding the third one.

^{232}Th decays into ^{208}Pb through a chain of six α decays and four β decays. In secular equilibrium, the complete network includes five β-decaying nuclei. Only two nuclides (^{228}Ac and ^{212}Bi) yield antineutrinos with energy larger than 1.806 MeV. The thorium contribution to the geo-neutrino signal comes from three β decays: one from ^{212}Bi and two from ^{228}Ac (see Table II). In fact, 94% of the thorium signal arises from the transition to the ground state of ^{212}Po (in bold in Table II).

We remind the reader that assuming the chondritic ratio for the global uranium and thorium mass abundances, $a(\mathrm{Th})/a(\mathrm{U}) = 3.9$, one expects that geo-neutrinos from uranium (thorium) will contribute about 80% (20%) of the total U + Th geo-neutrino signal. Current geo-neutrino measurements are weakly sensitive to $a(\mathrm{Th})/a(\mathrm{U})$ and are consistent[4] with the chondritic ratio [5].

In summary,

(i) Ninety-eight percent of the uranium geo-neutrino signal comes from just two transitions: one from ^{214}Bi and the other from ^{234}Pa. They provide 77% of the expected total U + Th signal.

(ii) A single decay of ^{212}Bi accounts for 94% of the thorium signal. It provides 20% of the expected U + Th signal.

Just three transitions have to be investigated experimentally. In this respect, the following considerations can be useful:

(i) ^{222}Rn ($\tau_{1/2} = 3.824$ days) can be easily dissolved in the scintillator, and the decay of ^{214}Bi is uniquely identified by the subsequent decay of ^{214}Po ($\tau_{1/2} = 164.3\ \mu$s).

[4]The best-fit value is much larger, about 7, but any ratio is consistent with data at the 1σ level. Because the ratio of the uranium to thorium contribution to the signal is directly proportional to $a(\mathrm{Th})/a(\mathrm{U})$, the effect on the relative contribution of a different ratio is easily obtained. For instance, a hypothetical large value $a(\mathrm{Th})/a(\mathrm{U}) = 7$ would make the relative contributions of uranium and thorium to the signal about 70% and 30%, respectively.

(ii) By dissolving ^{238}U in the scintillator, one can detect the β decay of ^{234}Pa (superimposed, however, with that of ^{234}Th). The subsequent decays of the chain are effectively blocked by the long half-life of ^{234}U ($\tau_{1/2} = 2.455 \times 10^5$ years).

(iii) For the investigation of ^{212}Bi decay, one has to start with a ^{224}Ra source ($\tau_{1/2} = 3.66$ days) or with a ^{232}Th source. The decay of ^{212}Bi can be easily identified by the subsequent α decay of ^{212}Po ($\tau_{1/2} = 299$ ns).

VI. RESULTS FROM A DIFFUSE RN SOURCE

To test the method that we are proposing, we have used data from a sizable, though limited, radon contamination of CTF, which occurred in the early phase of operation of the detector.[5] In the full volume of CTF, we selected candidate β decays from ^{214}Bi by the distinctive subsequent ^{214}Po α decay, which occurs with a mean time delay of 237 μs (the so-called Bi-Po events). The selection of the analyzed events (see the data points in Fig. 5) is described in Secs. VI A and VI B.

We recall that most of the contribution to the geo-neutrino signal arises from the transition to the lowest energy state (0) of ^{214}Po (see Fig. 6). Our analysis aims

(i) to determine the probability p_0 of populating the lowest energy state (assuming the universal allowed shape) from the CTF data

(ii) to determine whether the spectrum of the pure β transition (that to the lowest state) is deformed with respect to the universal allowed shape

(iii) to discuss the implications of this study on the specific geo-neutrino signal $s(^{214}\text{Bi})$, given by Eq. (2).

[5]The initial event rate of the used data was about 10 s^{-1}.

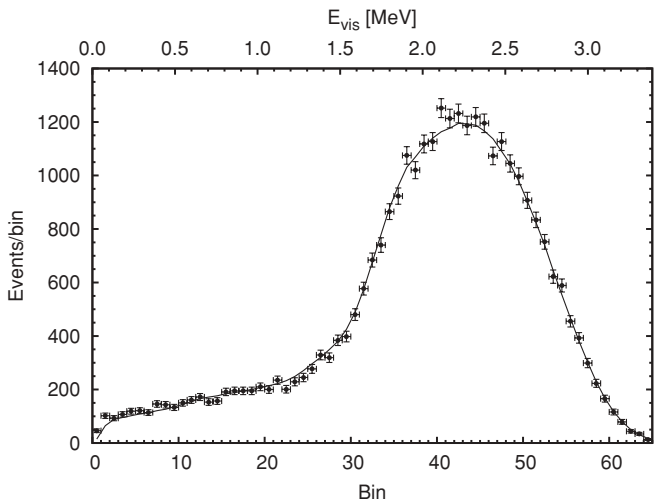

FIG. 5. Data and best fit. Events have been grouped into 65 bins from 0 to 3.4 MeV. Event numbers together with statistical error (vertical bar) and bin size (horizontal bar) are presented as a function of bin number (see text). We only fit data in bins from 3 to 65. The curve shows the best fit when three parameters (p_0, light yield, and normalization) are left as free.

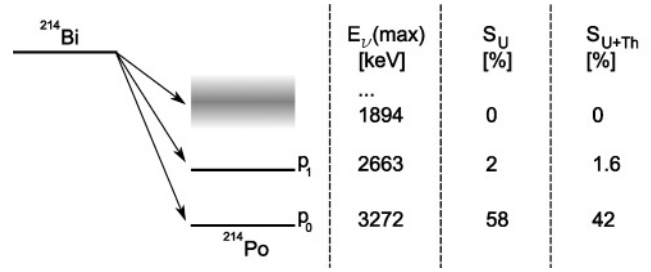

FIG. 6. A simplified decay scheme of ^{214}Bi and the contribution of the various levels to the total geo-neutrino signal.

A. Data selection and backgrounds

The main selection criterion is that the coincidence time between consecutive signals, provided by the prompt β decay of ^{214}Bi and the delayed α decay of ^{214}Po, be $2\ \mu\text{s} < \Delta t_{1/2} < 602\ \mu\text{s}$. The lower limit eliminates fast coincidences from the corresponding decays in the ^{232}Th chain, whereas the higher limit has been chosen to keep random coincidences under 1%, while preserving high statistics. The selected events are 4.54×10^5.

Then we require that the energy deposited by the first signal is $E_1 < 3.9$ MeV, taking into account the Q value ($Q = 3.27$ MeV) and the energy resolution, about 0.2 MeV at these energies. This cut removes random coincidences, while keeping the Bi-Po events (acceptance almost 100%).

The reconstructed radial positions[6] of the two signals r_1 and r_2 are used to impose the three conditions: $r_1 < 2$ m, $r_2 < 2$ m, and $|r_1 - r_2| < 2.5$ m. These very weak cuts have total acceptance efficiency of about 100%, while removing random coincidences.

We then impose that the energy of the second signal, on the electron energy scale, is $0.56\ \text{MeV} < E_2 < 1.1$ MeV (note that the amount of light produced by the 7.9-MeV α particles from ^{214}Po decay is quenched by a factor of about 11) to reduce low-energy αs of the Rn chain and random coincidences. The acceptance efficiency is 98.7%.

CTF has good pulse-shape discrimination between α and β events [15]. To avoid contamination of the $\beta + \gamma$ spectrum by high-energy αs, we add cuts on a suitable α/β discrimination parameter. The combined acceptance efficiency is 99.4%, and we are left with 4.46×10^5 events.

The remaining background is estimated by applying the same sets of cuts with the coincidence time window of $2000\ \mu\text{s} < \Delta t_{1/2} < 8000\ \mu\text{s}$. In this way, we estimate that contamination of random coincidences is about 0.7%.

B. Data analyses and fiducial region

Taking into account the number of events and the estimated energy resolution $\Delta E \approx 80\ \text{keV} \times (E/\text{MeV})^{1/2}$, we grouped events in bins of about 50 keV[7] and analyzed the 63 bins

[6]A typical spatial 1σ resolution is of order 10 cm at 1 MeV.

[7]The energy scale depends on the best-fit value of the light yield. At the best fit, the bin size is 52 keV.

from 0.1 up to 3.4 MeV. We checked that increasing the lower threshold to 0.15 or 0.2 MeV gives consistent results.[8]

To reduce systematic effects because of γs that are only partially contained and because of deviations from spherical symmetry, one should select events near the detector's center. On the other hand, statistics improve with increasing volume. We found that a good compromise is to consider events such that the αs' reconstructed positions are within a sphere of 42 cm around the CTF center. This sphere, after the cuts discussed earlier, contains 3.14×10^4 candidate decays.

The theoretical spectra have been produced with the CTF code described in Ref. [14] and with the specific adjustments presented in the appendix. Detector response functions and efficiencies are reproduced by the MC code and experimentally tested with the β spectrum from ^{14}C and known αs from the radon chain [13]. Indeed, the spectrum is precise enough to test the shape of the β spectrum even at low energies [16].

C. Feeding probability of the lowest state

First we shall assume that the neutrino energy distribution $f(E_\nu)$ is given as a sum of universal functions, that is,

$$f(E_\nu) = \sum_n p_n F_{\text{univ}}(E_\nu, Q - E_n), \tag{8}$$

where E_n is the energy of the nth level ($E_0 = 0$); that is, the maximal energy that can be taken by the neutrino is $Q - E_n$, and the functions $F_{\text{univ}}(E_\nu, Q - E_n)$ are each normalized to unity. The electron kinetic-energy distribution is

$$\phi(T_e) = \sum_n p_n \Phi_{\text{univ}}(T_e, Q - E_n). \tag{9}$$

The universal distributions for neutrinos and electrons are related by

$$\Phi_{\text{univ}}(T_e, Q - E_n) = F_{\text{univ}}(E_\nu = Q - E_n - T_e, Q - E_n). \tag{10}$$

The populations of the 82 excited ^{214}Po states are fixed at the values given in the table of isotopes (ToI) [17] apart from a common normalization factor such that the total population of these states is $(1 - p_0)$. This assumption for the excited states means that the relative intensities of the γ transition lines in the decay are exactly determined.

We fitted the data with Monte Carlo-generated spectra, leaving as free parameters the following:

(i) p_0, the feeding probability of the lowest state
(ii) the light yield L, defined as the number of photoelectrons that would be collected by 100 photomultipliers for an electron depositing 1 MeV at the center of the CTF

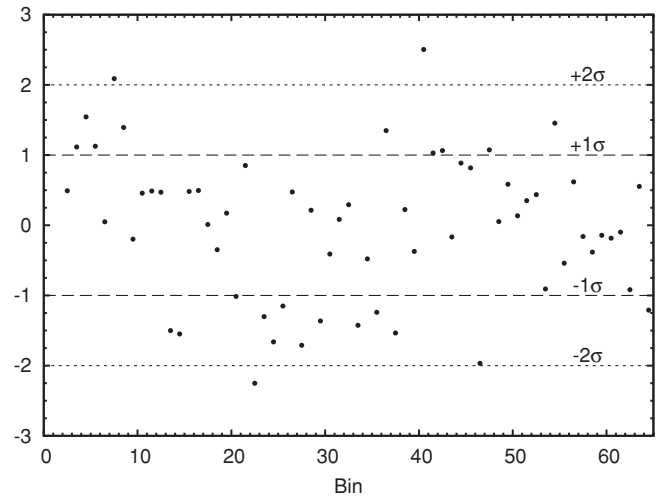

FIG. 7. Data and best fit: residuals. The values shown are the residuals relative to Fig. 5: data minus best-fit value divided by the square root of data. The best fit is obtained with three parameters (p_0, light yield, and normalization) left as free for data in bins from 3 to 65.

(iii) the normalization, that is, the number of reconstructed candidates (which should be equal to the number of candidates).

The best-fit function and the residuals are shown in Figs. 5 and 7. At the minimum χ^2/degrees of freedom $= 61.7/(63 - 3)$, the light yield $L = 321$ pe/MeV,[9] and the normalization factor is 0.998. The best-fit value is $p_0 = 0.177$, with a statistical 1σ error of ± 0.004.

Systematic uncertainties arise from limitations of the Monte Carlo simulation with respect to the real detector (see the appendix). We found that the largest uncertainties originate from the imperfect spherical symmetry of the detector, arising because of the deformations of the inner vessel (IV), and from nonuniform distribution of the active PMTs. The nature of these systematic errors makes them more important for events at large radii or involving high-energy γs, which can deposit energy far away from the point of origin. Therefore we estimated the effect of these errors on our measurements by analyzing a subgroup of events with different distance r from the center of the detector. Results show a consistent behavior as a function of r. Effects of the uncertainties on the quenching parameters, subtraction of random coincidences, selection of the energy window, and choice of the size of the energy binning have also been considered. In conclusion, the total systematic error is estimated as $^{+0.003}_{-0.001}$ so that

$$\text{(CTF)} \quad p_0 = 0.177 \pm 0.004\ (\text{stat})\ ^{+0.003}_{-0.001}\ (\text{sys}). \tag{11}$$

This value is consistent with that reported in ToI [17]: $p_0(\text{ToI}) = 0.182 \pm 0.006$.

[8]Given the importance of knowing the energy dependence of the detector response for our measure, we did not lower the threshold below 100 keV, because only above 100 keV the energy scale is sufficiently linear that corrections from calibrations are very reliable.

[9]Note that this light yield is within 3% of the one determined at much lower energy by a fit to ^{14}C events.

D. Shape factor for the pure β transition

Next we release the assumption that the spectrum for the transition to the ground state, which is a first forbidden transition, has the universal shape. The electron energy distribution is assumed to be

$$\phi(T_e) = p_0\Phi(T_e) + \sum_{n>0} p_n\Phi_{\rm univ}(T_e, Q - E_n), \qquad (12)$$

where

$$\Phi(T_e) = \Phi_{\rm univ}(T_e, Q)\left(1 + y\frac{T_e - \langle T_e\rangle}{\langle T_e\rangle}\right) \qquad (13)$$

and the average energy $\langle T_e\rangle$ is calculated over $\Phi_{\rm univ}(T_e, Q)$.

The dimensionless shape parameter y thus describes a deviation from the universal formula. Note that this simple parametrization does not change the normalization of the distribution; it only changes its shape. Other parametrizations are, of course, possible.[10] Shape and intensities of the excited states could also be allowed to change, but signal from these states is only background for this measure, and its knowledge is only needed at low energy as corrections to the ideal detector (see Fig. 1). At the level of the accuracy of this preliminary study, our conclusions do not change; that is, these effects are much smaller than the present uncertainties because of detection of higher energy γs (see the appendix).

The present data do not allow us to independently determine p_0, p_1, and y. We therefore consider as inputs the values given in ToI, $p_0 = 0.182 \pm 0.006$ and $p_1 = 0.017 \pm 0.006$ (we added two penalty factors to the χ^2 with errors assumed uncorrelated), and leave only y as an unconstrained parameter. The resulting χ^2 is shown in Fig. 8 as a function of y. At the best fit, we find χ^2/degrees of freedom $= 51.6/(65 - 5)$, $p_0 = 0.177$, $p_1 = 0.008$, and

$$y = -0.11 \pm 0.06\ (\text{stat}). \qquad (14)$$

The universal spectrum, $y = 0$, has a χ^2 larger by 5.9 with respect to the minimum. If both p_0 and p_1 are left completely unconstrained (no penalty factors), one again finds that the best-fit value for y is -0.11, but with a larger 1σ interval: $-0.53 < y < -0.09$. However, spectral deformation is very sensitive to the lowest part of the visible energy, and therefore we expect larger systematic uncertainties than the one estimated in the case of p_0. In fact, the analysis of a subgroup of events with different distances from the center of the detector, as we analyzed for the feeding probabilities, results in an estimated systematic error for y of the same size of its deviation from zero, that is, $\approx$0.10. Therefore the deviation from the universal spectrum is within 1σ from zero when present systematics is included.

Our present result only shows that the method is sensitive to the form of the spectrum and has the potentiality of detecting spectral deformations. However, interesting results can be obtained by achievable reductions of statistical and systematic errors. A large improvement will be obtained by positioning suitable sources near the center of the detector.

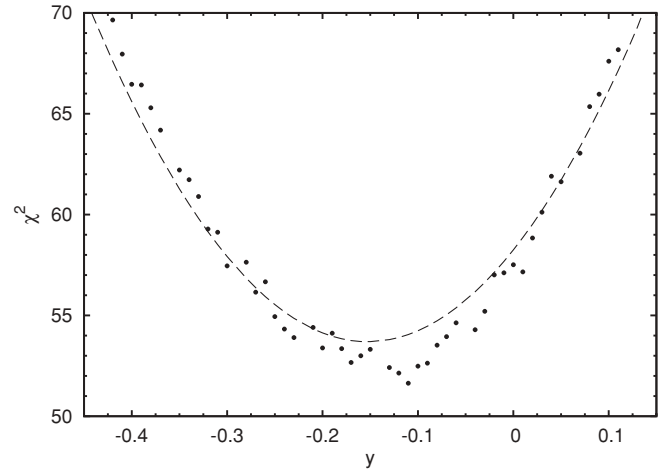

FIG. 8. The χ^2 as a function of the deformation parameter y. The number of degrees of freedom is (65–5).

E. Implications for the specific signal

The geo-neutrino signal $s(^{214}\text{Bi})$ can be written as the sum of two contributions:

$$s(^{214}\text{Bi}) = p_0\langle\sigma\rangle_0 + p_1\langle\sigma\rangle_1, \qquad (15)$$

where the cross section of reaction Eq. (1) is averaged over the neutrino energy distribution. Assuming universal shape, that is, $\langle\sigma\rangle_0 = \int dE_\nu\sigma(E_\nu)F_{\rm univ}(E_\nu, Q - E_n)$, the cross sections are $\langle\sigma\rangle_0 = 7.76$ and $\langle\sigma\rangle_1 = 2.825$ in units of 10^{-44} cm^2, with errors of an order of half a percent. Clearly the largest contribution to the geo-neutrino signal is given by the first term in Eq. (15) so that the relative error is practically the one on p_0. From the previous analysis, we find that

(CTF)
$$s(^{214}\text{Bi}) = [1.42 \pm 0.03\ (\text{stat})\ ^{+0.023}_{-0.008}\ (\text{sys})] \times 10^{-44}\ \text{cm}^2. \qquad (16)$$

This should be compared with the result derived using the ToI:

(ToI)
$$s(^{214}\text{Bi}) = [1.46 \pm 0.05\ (\text{stat})] \times 10^{-44}\ \text{cm}^2. \qquad (17)$$

If spectral distortion is allowed in the form of Eq. (13), then $\langle\sigma\rangle_0$ becomes

$$\langle\sigma\rangle_0 \to \langle\sigma\rangle_0 + y\langle\Delta\sigma\rangle_0, \qquad (18)$$

where $\langle\sigma\rangle_0 = 7.76$ and $\langle\Delta\sigma\rangle_0 = -4.52$.

If we substitute the value of y in Eq. (14) and the corresponding values for $p_0 = 0.177$ and $p_1 = 0.008$, we find that

$$s(^{214}\text{Bi}) = [1.48 \pm 0.01\ (\text{stat}) \pm 0.03\ (\text{sys})] \times 10^{-44}\ \text{cm}^2. \qquad (19)$$

[10]Physically, the leading corrections from nuclear matrix elements to the spectral shape are proportional to the square of the momentum of the electron p_e and of the neutrino p_ν. Given that $p_\nu = Q - T_e$, at low energy, the main effect can be effectively described with only one parameter: the coefficient of the electron kinetic energy T_e.

Note that if we leave completely unconstrained the shape p_0, p_1, and y, the effects of changes of shape and of p_0 on the signal are anticorrelated: If the spectrum is deformed so that there are more (less) low-energy electrons, the corresponding best-fit value for p_0 is lower (higher). For instance, using the present parametrization, we can let y span from -0.64 to 0.13, finding the corresponding best-fit values for p_0 and p_1 with no constraint (we disregard the fact that these best-fit values often have too-large χ^2): While the values of p_0 go from 0.13 to 0.20, the signal changes only by about $\pm 2\%$. In other words, the resulting signal is weakly dependent on the shape factor.

VII. CONCLUDING REMARKS

So far, we have estimated the ^{214}Bi geo-neutrino specific signal by using CTF data resulting from a limited radon contamination. Our estimate has a comparable error with that derived from ToI [see Eqs. (16) and (17)]. We remark, however, that our method has two advantages:

(i) The pure β transition can be detected in CTF and its probability can be measured directly (whereas in the study of γ lines alone, its existence was inferred from the fact that the γ counts did not match with the expected number of decays, and the probability was evaluated from this mismatch).
(ii) One can check the validity of the universal shape approximation for the most important decay mode.

A dedicated experiment makes sense, with the aim of reducing the relative statistical error $\Delta p_0/p_0$ to the level of the relative error on the cross section, $\Delta\langle\sigma\rangle_0/\langle\sigma\rangle_0 \approx 0.5\%$. This requires a statistics larger by a factor of about 20 or some 6×10^5 selected events. At the same time, one has to reduce systematic errors in the correspondence between measured light and released energy: The largest improvement should be obtained by concentrating the source near the center of the detector.

Our preliminary results are of encouragement toward a series of dedicated measurements, with suitable sources dissolved in the liquid scintillator and placed in a vial near the CTF center. As an example, a ^{222}Rn source with an initial activity of 5 Bq would be tolerable for CTF and would produce some 2×10^6 decays in 11 days (two lifetimes). Electrons are stopped inside the vial, and the scintillation light is propagated within CTF through the quartz, whereas γ conversion occurs inside the CTF inner vessel. The inward-facing PMTs outside the shroud can thus detect light originating from both electrons and γs. Along these lines, one can get a better estimate of the specific signal of ^{214}Bi; provide measurements of the other signals, $s(^{234}\text{Pa})$ and $s(^{212}\text{Bi})$, relevant for geo-neutrino studies; and more generally, measure the energy spectra of neutrinos from long-lived heavy nuclei.

ACKNOWLEDGMENTS

We are grateful for enlightening discussions with and the valuable comments of E. Bellotti, G. Bellini, B. Ricci, and C. Tomei. We thank the Borexino Collaboration for providing data. This work was partially supported by Ministero dell'Istruzione, dell'Università e della Ricerca under MIUR-PRIN-2006 Project "Astroparticle Physics."

APPENDIX: MONTE CARLO SIMULATION OF CTF DETECTOR

Because light propagation in a large-volume scintillator detector involves complex mechanisms, the precise modeling of the detector response requires that many phenomena be taken into account. Among the most relevant issues, it is worth mentioning the wavelength dependence of the processes involved in light propagation, the reflection and refraction at the scintillator-water interface, and the light reflection on the concentrators. The need to follow each of some 12,000 photons emitted per 1-MeV electron event makes tracing Monte Carlo code very slow.

A fast and reliable code has been developed for the CTF detector and is briefly described in this appendix (more details can be found in Ref. [14]). The code takes advantage of using average parameters (such as light yield, energy resolution, and spatial reconstruction precision) obtained analyzing the detector's data. Optimal sets of data for calibrating, tuning, and testing the code are the β-decay spectrum from ^{14}C and the easily identifiable αs from the radon-chain decays. The code has two parts: the electron-γ shower simulation (EG code) and the simulation of the registered charge and position (REG code).

The EG code generates events at a random position with random initial direction (for γs) and follows the electron-γ shower using the EGS-4 code [18]. The low-energy electrons and αs are not propagated in the program and are considered to be pointlike sources, located at the initial coordinates. The mean registered charge corresponding to the electron kinetic energy T_e is calculated with

$$Q_e(r) = A \cdot T_e \cdot f(k_B, T_e) f_R(r), \tag{A1}$$

where $f_R(r)$ is a radial factor that takes into account the dependence of the registered charge on the distance from the detector's center and $f(k_B, T_e)$ is the ionization quenching factor for electrons; the normalization of these two factors has been chosen such that $f_R(0) = f(k_B, T_e = 1\ \text{MeV}) = 1$. The method used to obtain $f_R(r)$ consists of studying the response for monoenergetic αs as a function of their radial position and is described in Ref. [19].

For the liquid scintillator, consisting of a binary mixture of pseudocumene (1,2,4-trimethylbenzene or PC) as solvent and PPO (2,5-diphenyloxazole) as primary fuor (PC + PPO 1.5 g/l), the quenching factor $k_B = (1.7 \pm 0.1) \times 10^3$ cm MeV^{-1} was found to satisfy experimental data [20]. This value agrees with the fit to the high-statistics β spectrum of ^{14}C. The α particles from ^{214}Po decay, which tag the Bi-Po events considered in our study, have an energy of 7.69 MeV and are quenched to an equivalent β energy (they produce the same amount of light in the scintillator of an electron) of 751 ± 7 keV. In the set of data selected for this article, quenching was higher (and the light yield lower) than in Ref. [20] because of the presence of oxygen in the scintillator (the radon originated from atmospheric air). In fact, the 7.69-MeV αs are found

at the lower equivalent β energy, $E = 643$ keV, for events selected around the detector's center. The ratio of two energies can be used to scale the quenching k_B factor: The adopted value is $k_B = 0.0195$ cm MeV^{-1}.

The γs are propagated using the EGS-4 code. As soon as the ith electron of energy T_{e_i} appears inside the scintillator, the corresponding fraction of total registered charge is calculated:

$$\Delta Q_i = A \cdot T_{e_i} \cdot f(k_B, T_{e_i}) f_R(r_i). \tag{A2}$$

The total mean collected charge is defined when the γ is discarded by the EG code as the sum of the individual deposits:

$$Q_\gamma = \sum_i \Delta Q_i. \tag{A3}$$

The weighted position is assigned to the final γ:

$$\mathbf{r}_w = \frac{\sum_i \Delta Q_i \cdot \mathbf{r}_i}{\sum_i \Delta Q_i}, \tag{A4}$$

where ΔQ_i is the charge deposited by the ith electron at the position $\mathbf{r}_i$.

Once the position and deposited charge of the event have been generated by the EG code as described earlier, the second part of the code (REG) randomly generates the corresponding number of photoelectrons registered at each PMT; it takes into account the proper geometrical factor and assumes Poissonian distributions of photoelectron numbers at each PMT.

Finally, the energy-dependent radial reconstruction is simulated. The reconstruction precision is assumed to be defined by the number of PMTs fired and is dependent only on the distance from the detector's center (spherical symmetry). These two assumptions have been confirmed by measurements using artificial radon sources inserted in the CTF detector [13,21].

The main source of systematic errors in our study is the departure from spherical symmetry of the detector because of deformations of the IV and nonuniform distribution of active PMT on the spherical surface surrounding the scintillator. The IV, a 500-μm-thick nylon bag containing 4 tons of low-density ($\approx$0.88 g/cm^3) scintillator, is immersed in water. The buoyancy forces are compensated by supporting strings, but the deformations are not measured precisely and are not accounted for in the Monte Carlo modeling. The maximum radial deviations from the ideal sphere can be as big as from 5 to 10 cm, though on average, the radius of the sphere is $R = 100$ cm. Another source of systematics of the same nature (absent in an ideal spherical detector) is the position dependence of the light-collection efficiency function, $f_R(r)$, which is assumed to depend only on the distance from the center and not on all three coordinates. The nature of these systematic errors makes them more important for events at large radii or involving high-energy γs, which can deposit energy far away from the point of origin.

[1] F. Mantovani, L. Carmignani, G. Fiorentini, and M. Lissia, Phys. Rev. D **69**, 013001 (2004).
[2] G. L. Fogli, E. Lisi, A. Palazzo, and A. M. Rotunno, Earth Moon Planets **99**, 111 (2006).
[3] S. Enomoto, E. Ohtani, K. Inoue, and A. Suzuki, Earth Planet. Sci. Lett. **258**, 147 (2007).
[4] G. Fiorentini, M. Lissia, F. Mantovani, and R. Vannucci, Phys. Rev. D **72**, 033017 (2005).
[5] T. Araki *et al.* (KamLAND Collaboration), Nature **436**, 499 (2005).
[6] S. Abe *et al.* (KamLAND Collaboration), Phys. Rev. Lett. **100**, 221803 (2008).
[7] G. Alimonti *et al.* (Borexino Collaboration), Astropart. Phys. **16**, 205 (2002).
[8] G. Alimonti *et al.* (Borexino Collaboration), Nucl. Instrum. Methods A **600**, 568 (2009).
[9] G. Fiorentini, M. Lissia, and F. Mantovani, Phys. Rep. **453**, 117 (2007).
[10] P. Vogel and J. F. Beacom, Phys. Rev. D **60**, 053003 (1999).
[11] A. Strumia and F. Vissani, Phys. Lett. **B564**, 42 (2003).
[12] C. Bucci and P. Gorla (private communication).
[13] G. Alimonti *et al.*, Nucl. Instrum. Methods A **406**, 411 (1998).
[14] H. O. Back *et al.* (Borexino Collaboration), Eur. Phys. J. C **37**, 421 (2004).
[15] H. O. Back *et al.* (Borexino Collaboration), Nucl. Instrum. Methods A **584**, 98 (2008).
[16] G. Alimonti *et al.* (Borexino Collaboration), Phys. Lett. **B422**, 349 (1998).
[17] Y. A. Alkovali, Nucl. Data Sheets **76**, 127 (1995).
[18] W. R. Nelson, H. Hirayama, and D. W. O. Rogers, Report No. SLAC-265, National Accelerator Laboratory, Menlo Park, CA 1985 (unpublished).
[19] A. Derbin, A. Ianni, V. Muratova, and O. Smirnov (Borexino Collaboration), Borexino Internal Note, 2003 (unpublished).
[20] G. Bellini *et al.* (Borexino Collaboration), Eur. Phys. J. C **54**, 61 (2008).
[21] K. B. McCarty, Ph.D. thesis, Princeton University, 2006.